



Coburn, B. H., & Weaver, P. M. (2016). Buckling analysis, design and optimisation of variable-stiffness sandwich panels. *International Journal of Solids and Structures*, 96, 217-228.  
<https://doi.org/10.1016/j.ijsolstr.2016.06.007>

Peer reviewed version

License (if available):  
CC BY-NC-ND

Link to published version (if available):  
[10.1016/j.ijsolstr.2016.06.007](https://doi.org/10.1016/j.ijsolstr.2016.06.007)

[Link to publication record in Explore Bristol Research](#)  
PDF-document

This is the author accepted manuscript (AAM). The final published version (version of record) is available online via Elsevier at <http://www.sciencedirect.com/science/article/pii/S002076831630124X>. Please refer to any applicable terms of use of the publisher.

## University of Bristol - Explore Bristol Research

### General rights

This document is made available in accordance with publisher policies. Please cite only the published version using the reference above. Full terms of use are available:  
<http://www.bristol.ac.uk/red/research-policy/pure/user-guides/ebr-terms/>

# Buckling analysis, design and optimisation of variable-stiffness sandwich panels

Broderick H. Coburn<sup>a,\*</sup>, Paul M. Weaver<sup>a</sup>

<sup>a</sup>*Advanced Composites Centre for Innovation and Science, University of Bristol, Queen's Building, Bristol BS8 1TR, United Kingdom*

---

## Abstract

In recent years variable-stiffness (VS) technology has been shown to offer significant potential weight savings and/or performance gains for both monolithic and stiffened plate structures when buckling is a driving consideration. As yet, little work has been reported on VS sandwich structures. As such, a semi-analytical model is developed based on the Ritz energy method for the buckling of sandwich panels with fibre-reinforced VS face-sheets. The model captures both global and shear crimping instabilities and is shown to be accurate and computationally efficient compared to commercial two- and three-dimensional finite element analyses. Subsequent parametric and optimisation studies, which were performed for many practical geometries using the developed model, reveal that, whilst VS sandwich panels show a significant improvement in global buckling performance, they suffer a reduction in shear crimping performance when compared to their straight-fibre counterparts. This behaviour is found to be due to the VS face-sheets creating a pre-buckling load redistribution where regions locally exceed the critical shear crimping load and induce the short wavelength instability at a reduced panel level load. For VS sandwich panels with modest to low transverse shear moduli of the core, shear crimping can become the critical mode diminishing performance benefits relative to straight-fibre configurations. Cores with sufficient flexural rigidity, thus preventing shear crimping, showed improvements in critical buckling load in the order of 80 % when using VS, however this improvement reduces to a negligible amount with decreasing core transverse shear moduli. The transverse shear flexibility and load redistribution are thus two key parameters that must be considered carefully in the design of sandwich panels, in order to exploit the benefits of VS fully in this novel structural configuration. *Keywords:* Fibre-steering, Ritz method, Shear crimping, Transverse shear, Variable-angle tow

---

## 1. Introduction

Traditional tailoring of fibre-reinforced composites is achieved by varying the orientation of fibres through the thickness of a laminate. However, recent advancements of automated fibre placement (AFP) and tape

---

\*Corresponding author

Email address: broderick.coburn@bristol.ac.uk (Broderick H. Coburn)

laying technologies have led to the possibility of steering fibres in the plane of a ply, thus creating variable-stiffness laminates and significantly increasing the design space available to engineers. In recent times, performance benefits of VS laminates have been shown for: the buckling and post-buckling of plates [1–7], shells [8] and stiffened panels [9–11]; the stress distribution around discontinuities [12, 13]; and stiffness blending of structures [14, 15]. The manufacture of VS laminates has been achieved largely through the established AFP [14] and lately through an early concept manufacturing method called continuous tow shearing [16, 17].

The majority of work to date on the buckling of VS structures is limited to simple configurations, such as plates and shells, with simple boundary conditions. Whilst analytical and semi-analytical methods [1, 2, 4] provide an accurate and computationally efficient alternative to finite element analysis (FEA), they are often limited to simple cases in terms of loading, boundary conditions, geometry and structural configuration. Recently, Coburn et al. [9, 10] developed an analytical model based on the Ritz energy method for the buckling of stiffened VS panels including a first-order shear deformation theory (FSDT) to enable the study of thick laminate sections. Using the model in a follow-up optimisation study [11], it was shown that stiffened VS panels can achieve mass reductions when compared to straight-fibre stiffened panels, albeit to a lesser extent than plates considered in isolation [1, 3, 4, 18].

One application of VS that has not been explored to date, to the best of the authors’ knowledge, is the use of fibre-steering in composite face-sheets to create VS sandwich panels. Sandwich panels are well known to be efficient structures in bending and buckling and for this reason are commonly used in regions where supported edges are spaced far apart. The aim of this work is to use the approach presented by Coburn et al. [10], including a FSDT in a semi-analytical Ritz model, to explore structural configurations of VS sandwich panels and the effect of fibre-steering and core shear flexibility on buckling performance. In particular, the study will focus on translating the case identified by Gürdal and co. [1, 18], who showed that a simply-supported square plate subject to uniform end-shortening can achieve up to 80% improvement in critical buckling load with a lateral direction fibre path variation, to sandwich panels. **We found that the simple FSDT was of sufficient fidelity to understand and explain the response of the sandwich panels we consider. Future work could consider development of models, such as that recently developed by Groh and Weaver [19], which could represent the behaviour of more general sandwich panels that could be thicker or have more complex boundary conditions and loading.**

The following sections are structured as follows: Section 2 develops a **two-dimensional** semi-analytical model for the buckling analysis of VS sandwich panels subject to uniaxial and biaxial loading with clamped and simply-supported boundary conditions **applying a FSDT**; a parametric study is then performed in Section 3 on the fibre angle variation for panels with various core properties, followed by a discussion of the failure modes and significance of core shear stiffness; in Section 4, an optimisation study with an increased variation in fibre-steering is performed identifying optimal configurations and improvements; and finally, the

paper is concluded in Section 5.

## 2. Semi-analytical model

The semi-analytical model considers uniaxial and biaxial loading of a prismatic sandwich panel with fibre-steering in the lateral direction ( $y$ -direction). Previous studies on VS plates [18] indicate that a one-dimensional variation, perpendicular to the principal loading direction leads to a favourable redistribution of loads towards supported boundaries, improving the global buckling performance and additionally allowing manufacturable fibre paths. The extension of the model to fibre paths varying in the longitudinal direction or in-plane shear loading could be achieved with the use of a more generalised **Airy stress function** and the pre-buckling boundary conditions as detailed in Wu et al. [20].

Transverse shear strains are included in the analysis with a through thickness weighted average approach, as is typically the case with a FSDT. FSDTs [21–23] can provide accurate solutions with low computational cost for moderately thick plates and have previously been incorporated into the buckling analysis of thick plates and sandwich structures by applying the Ritz method and assuming additional shape functions for either rotation or transverse shear strain profiles [24–26]. Smearing properties and idealising the three-dimensional structure in two-dimensions, the FSDT is suitable for predicting global events such as buckling. For structures exhibiting large variations in stiffness through the thickness, such as sandwich panels, care must be taken when interpreting results obtained from a FSDT. It is acknowledged that for characteristic length to thickness ratios less than typically 20:1, or the requirement for detailed through thickness stresses, the FSDT approach detailed herein could be insufficient and higher-order shear deformation theories or full three-dimensional analyses would be required. The characteristic length of a panel, for the purposes of buckling analyses, is the dimension which drives the size of the buckling half-waves. For the case of long panels with edges free to expand, as is the case for the parametric and optimisation studies presented herein, this is typically the panel’s shorter transverse dimension. The characteristic length to thickness ratio provides a rule-of-thumb guide to the importance of through-thickness behaviour, as the characteristic length is a measure of the length over which a buckled half-wave occurs. Thus a more appropriate value for characteristic length, would therefore be the shortest dimension of the buckling half-waves that form, this however requires knowledge of the solution, and for pre-analysis guidance, appropriate panel dimension are therefore commonly used.

In this study the semi-analytical model was implemented in MATLAB R2013a [27].

### 2.1. Sandwich panel description and loading

The sandwich panel considered consists of two identical VS composite face sheets, individually constrained to be balanced and symmetric about their local geometric midplane ( $\mathbf{B}, A_{16}, A_{26} = 0$ ), either side

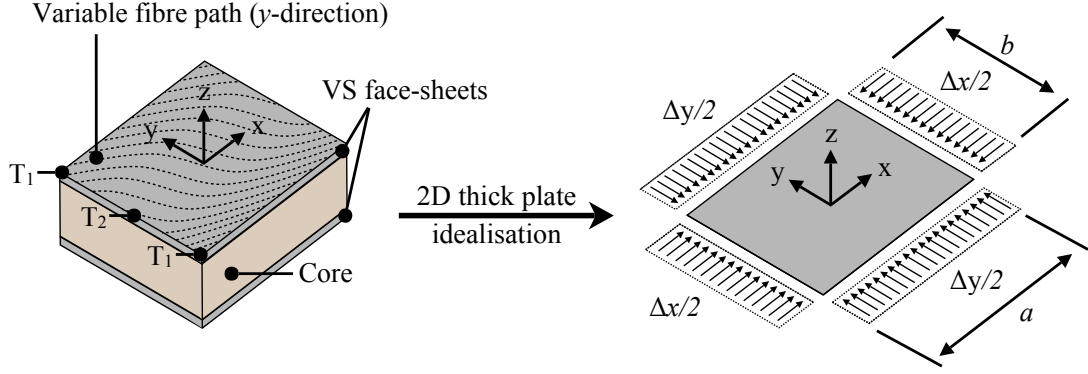


Figure 1: VS sandwich panel idealisation as a Mindlin-Reissner plate with loading, dimensions and the global coordinate system shown.

of a homogeneous orthotropic core material as shown in Figure 1. The sandwich panel is prismatic in loading, boundary conditions, and properties, with the fibre-steering restricted to the lateral direction of the laminates ( $y$ -direction). The panel is subject to uniaxial and biaxial uniform end-shortening.

## 2.2. Skin fibre path representation

Several definitions for the fibre variation over the plane of a laminate have been proposed in the literature, ranging from simple linear variations [1] to more complex higher-order variations [4]. Here, the piecewise linear method [28] is used due to its ease of visualisation and immunity to Runge's phenomenon [29]. The fibre angle in the  $y$ -direction is given by:

$$\theta(y) = \begin{cases} \theta_{1,2}(y) & \text{if } y_1 \leq y < y_2 \\ \theta_{2,3}(y) & \text{if } y_2 \leq y < y_3 \\ \dots & \\ \theta_{n-1,n}(y) & \text{if } y_{n-1} \leq y < y_n \end{cases} \quad (1)$$

where

$$\theta_{i,i+1}(y) = \left( \frac{T_i - T_{i+1}}{y_i - y_{i+1}} \right) y + \frac{T_{i+1}y_i - T_i y_{i+1}}{y_i - y_{i+1}};$$

$T_i$  and  $T_{i+1}$  are the  $i^{\text{th}}$  and  $(i^{\text{th}}+1)$  control point fibre orientations respectively; and  $y_i$  and  $y_{i+1}$  are the global coordinate system  $y$ -positions of the  $i^{\text{th}}$  and  $(i^{\text{th}}+1)$  control points respectively. A VS ply is designated by  $\langle T_1|T_2|\dots T_n \rangle$  for  $n$  control points whose positions are given by  $[y_1, y_2, \dots y_n]$ .

## 2.3. Formulation overview

The three-dimensional sandwich panel is idealised as a Mindlin-Reissner two-dimensional plate [22, 23], i.e. with transverse shear flexibility, as shown in Figure 1. Prior to the buckling analysis, a pre-buckling

analysis is required to determine the non-uniform stress resultant distribution in the VS structure when subject to uniform end-shortening. This is achieved using the approach of Wu et al. [4], albeit for the simpler prismatic case, by formulating the total complementary energy of the system and solving for the unknown **Airy stress function** with the Ritz method. For the buckling analysis, the total potential energy of the panel is given by contributions from the bending energy, transverse shear energy, and external work, and expressed as functions of the out-of-plane displacement and transverse shear strains. Applying the Ritz method by minimising the total potential energy yields an eigenvalue problem whose eigenvectors are the buckling modes.

#### 2.4. Stiffness matrices

For sandwich panels consisting of identical face-sheets and a core material (see Figure 1), the **A**-, **B**-, **D**-stiffness matrices about the global midplane are given by:

$$\begin{aligned} \mathbf{A} &= 2\mathbf{A}_{\text{fs}} + \mathbf{A}_{\text{c}}, & \mathbf{B} &= \mathbf{0}, & \text{and} \\ \mathbf{D} &= 2\mathbf{D}_{\text{fs}} + \frac{(h_{\text{fs}} + h_{\text{c}})^2}{2}\mathbf{A}_{\text{fs}} + \mathbf{D}_{\text{c}}, \end{aligned} \quad (2)$$

where  $h$  is a thickness, and the subscripts fs and c indicate a single face-sheet and the core respectively. **The A-matrix represents the extensional stiffness of the panel that relates in-plane forces to in-plane deformations, the B-matrix represents the in-plane-out-of-plane coupling stiffness of the panel that relates in-plane forces to curvatures, and moments to in-plane deformations, and the D-matrix represents the flexural stiffness of the panel that relates moments to curvatures.** Owing to the varying fibre orientation of the face-sheets all stiffness matrix terms are variable in the  $y$ -direction. The smeared transverse shear stiffness terms are determined using the approach detailed in Kollár and Springer [30] where the face-sheets are assumed to be thin, i.e. negligible stiffness in bending about their own midplane, and have a high transverse shear stiffness compared to the thick core. **The resulting transverse shear stress profile in the  $z$ -direction under these assumptions consists of a large and approximately constant transverse shear stress in the thick core region which ramps down, approximately linearly, in the thin skins to zero at the upper and lower surfaces [31].** Assuming the transverse shear deformation to be negligible in the face-sheets (high transverse shear stiffness) and constant in the core, the equivalent transverse shear stiffness of the sandwich plate can be given solely by core stiffness properties as:

$$H_{ij} = h_e \bar{Q}_{c,ij} \quad \text{where} \quad h_e = \frac{(h_{\text{fs}} + h_{\text{c}})^2}{h_{\text{c}}} \quad (3)$$

and is the equivalent core thickness for transverse shear rigidity purposes,  $i, j = 4, 5$ , and  $\bar{Q}_{c,ij}$  is the core stiffness matrix in the global coordinate system. For an orthotropic sandwich core, as is most commonly the case for foam and honeycomb constructions, the stiffness matrix in the local coordinate system,  $\mathbf{Q}_{\text{c}}$ , is

given by:

$$\mathbf{Q}_c = \begin{bmatrix} Q_{c,44} & Q_{c,45} \\ Q_{c,54} & Q_{c,55} \end{bmatrix} = \begin{bmatrix} C_{c,44} & C_{c,45} \\ C_{c,54} & C_{c,55} \end{bmatrix} = \begin{bmatrix} G_{c,23} & 0 \\ 0 & G_{c,13} \end{bmatrix}. \quad (4)$$

Full explanations of all stiffness and transformation matrices can be found in Reference [30]. **Ultimately, the assumptions made in the derivation of the smeared transverse shear stiffnesses for the sandwich panel limit the applicability of the model to skins which are thin and stiff in transverse shear relative to the core material. The use of thick skins would require the consideration of parabolic stress profiles in both the skins and core, whilst the use of shear flexible skins would invalidate the assumption of null transverse shear deformation in the skins. Therefore, sufficient care should thus be taken when using this approach outside of our assumptions.**

### 2.5. Pre-buckling

Two pre-buckling load cases are considered; in both cases the lateral edges are subject to a uniform end-shortening of  $\Delta x$  in the  $x$ -direction, with case A allowing longitudinal edges to expand, and case B additionally applying an end-shortening of  $\Delta y$  in the  $y$ -direction to create a biaxial stress state as shown in Figure 1. In both cases, all edges are free to translate parallel to the edge direction and the panel is constrained to have null  $A_{i6}$  ( $i = 1, 2$ ) extension-shear coupling terms resulting in either a purely uniaxial or biaxial stress state.

#### 2.5.1. Total complementary energy

The energy of the system for pre-buckling is formulated as the total complementary energy extending the approach of Wu et al. [20] who found that utilising the Ritz method for the pre-buckling problem of VS plates with prescribed edge displacements was intractable with the total potential energy. The total complementary energy of a plate subject to prescribed edge displacements is given by [20, 32]:

$$\begin{aligned} \Pi_c = & \frac{1}{2} \iint_S \left[ a_{11} \left( \frac{\partial^2 \Phi}{\partial y^2} \right)^2 + 2a_{12} \frac{\partial^2 \Phi}{\partial x^2} \frac{\partial^2 \Phi}{\partial y^2} + a_{22} \left( \frac{\partial^2 \Phi}{\partial x^2} \right)^2 \right. \\ & + a_{66} \left( \frac{\partial^2 \Phi}{\partial x \partial y} \right)^2 - 2a_{16} \frac{\partial^2 \Phi}{\partial y^2} \frac{\partial^2 \Phi}{\partial x \partial y} - 2a_{26} \frac{\partial^2 \Phi}{\partial x^2} \frac{\partial^2 \Phi}{\partial x \partial y} \Big] dy dx \\ & - \int_{-b/2}^{b/2} \left[ \frac{\partial^2 \Phi}{\partial y^2} u - \frac{\partial^2 \Phi}{\partial x \partial y} v \right]_{x=a/2} dy \\ & + \int_{-b/2}^{b/2} \left[ \frac{\partial^2 \Phi}{\partial y^2} u - \frac{\partial^2 \Phi}{\partial x \partial y} v \right]_{x=-a/2} dy \\ & - \int_{-a/2}^{a/2} \left[ \frac{\partial^2 \Phi}{\partial x^2} v - \frac{\partial^2 \Phi}{\partial x \partial y} u \right]_{y=b/2} dx \\ & + \int_{-a/2}^{a/2} \left[ \frac{\partial^2 \Phi}{\partial x^2} v - \frac{\partial^2 \Phi}{\partial x \partial y} u \right]_{y=-b/2} dx, \end{aligned} \quad (5)$$

where:  $a_{ij}$  ( $i, j = 1, 2, 6$ ) are the terms of the inverse of the in-plane stiffness matrix  $\mathbf{A}$ ;  $u$  and  $v$  are the displacements in the  $x$ - and  $y$ -directions respectively;  $S$  is the surface of the plate; and  $\Phi$  is the **Airy stress function** defined as:

$$N_x = \frac{\partial^2 \Phi}{\partial y^2}, \quad N_y = \frac{\partial^2 \Phi}{\partial x^2} \quad \text{and} \quad N_{xy} = -\frac{\partial^2 \Phi}{\partial x \partial y}, \quad (6)$$

where  $N_x$ ,  $N_y$  and  $N_{xy}$  are the in-plane stress resultants. The analysis is further simplified and generalised by expressing the total complementary energy in the normalised coordinate system of  $\xi$  and  $\eta$  with:

$$\xi = \frac{2x}{a} \quad \text{and} \quad \eta = \frac{2y}{b}. \quad (7)$$

### 2.5.2. Shape functions

Owing to the panel being prismatic the  $N_y$  stress resultant is constant over the entire domain and can be captured with a single term. By constraining the panel to have no extension-shear coupling or shear loading the  $N_{xy}$  stress resultant is null over the entire domain. The only variable stress resultant requiring representation with a series expansion is  $N_x$  which varies in the  $y$ -direction. The **Airy stress function**, in the normalised coordinate system (Equation 7), can therefore be represented as a polynomial series expansion given by:

$$\frac{\partial^2 \Phi}{\partial \eta^2} = \frac{b^2}{4} N_x = \sum_{h=1}^H [c_h L_{h-1}(\eta)] = c_h L_{h-1} \quad (8)$$

and

$$\frac{\partial^2 \Phi}{\partial \xi^2} = \frac{a^2}{4} N_y = d_0,$$

where  $L_{h-1}$  is the polynomial series in the  $y$ -direction,  $H$  the number of terms in the  $L_{h-1}$  series, and  $c_h$  the unknown coefficients. The variation in the  $y$ -direction,  $c_h L_{h-1}$ , is free at boundaries, with a Legendre polynomial series chosen for the  $L_{h-1}$  shape function. The use of polynomial series' enables the highly localised behaviour, present in VS structures, to be captured well due to the non-periodic nature of polynomials [4]. The total complementary energy of the system can then be expressed in terms of the unknowns,  $c_h$  and  $d_0$ , by substituting the shape functions, Equation 8, into the normalised form of Equation 5.

### 2.5.3. Principle of stationary complementary energy

Applying the principle of stationary complementary energy,  $\delta \Pi_c = 0$ , which is mathematically identical to the principle of stationary potential energy for linear systems, to the non-dimensional form of the total complementary energy and minimising with respect to the unknown coefficients results in a set of linear equations, which, expressed in matrix form, are given by:

$$\begin{bmatrix} \mathbf{U}_{cc} & \mathbf{U}_{cd_0} \\ \mathbf{U}_{cd_0}^T & \mathbf{U}_{d_0d_0} \end{bmatrix} \begin{bmatrix} \mathbf{c} \\ d_0 \end{bmatrix} = \begin{bmatrix} \mathbf{P}_{x0} \\ \mathbf{P}_{y0} \end{bmatrix}, \quad (9)$$



where, for example;  $\mathbf{U}_{cd_0}$  is the stiffness matrix of the  $\mathbf{c}$  coefficients obtained when minimising the total complementary energy of the system with respect to the  $d_0$  coefficient;  $\mathbf{P}_{x0}$  and  $\mathbf{P}_{y0}$  are the constants that arise when minimising the total complementary energy with respect to  $\mathbf{c}$  and  $d_0$  respectively; and  $\mathbf{c}$  and  $d_0$  a vector and scalar of the unknown coefficients respectively. The solution to the problem of Equation 9 yields the coefficients of the **Airy stress function** which enables the stress resultant field under the prescribed loading to be determined as per Equation 6.

## 2.6. Buckling

The Ritz method is used on the total potential energy to solve the buckling problem for the panel using the stress resultant distribution obtained in the pre-buckling analysis. The plate is loaded by the end-shortening  $\Delta x$  for pre-buckling case A and  $[\Delta x, \Delta y]$  for pre-buckling case B which is increased proportionally by a loading parameter,  $\lambda$ .

### 2.6.1. Total potential energy

The total potential energy of the panel is given by the sum of the bending strain energy,  $U_D$ ; transverse shear strain energy,  $U_H$ ; and external work,  $T$ , by:

$$\Pi = U_D + U_H + T, \quad (10)$$

where for a Mindlin-Reissner plate  $U_D$ ,  $U_H$  and  $T$  are given by [30]:

$$\begin{aligned} U_D = & \frac{1}{2} \int_{-a/2}^{a/2} \int_{-b/2}^{b/2} \left[ D_{11} \left( \frac{\partial^2 w}{\partial x^2} - \frac{\partial \gamma_{xz}}{\partial x} \right)^2 + D_{22} \left( \frac{\partial^2 w}{\partial y^2} - \frac{\partial \gamma_{yz}}{\partial y} \right)^2 \right. \\ & + 2D_{12} \left( \frac{\partial^2 w}{\partial x^2} - \frac{\partial \gamma_{xz}}{\partial x} \right) \left( \frac{\partial^2 w}{\partial y^2} - \frac{\partial \gamma_{yz}}{\partial y} \right) \\ & + D_{66} \left( 2 \frac{\partial^2 w}{\partial x \partial y} - \frac{\partial \gamma_{xz}}{\partial y} - \frac{\partial \gamma_{yz}}{\partial x} \right)^2 \\ & + 2D_{16} \left( \frac{\partial^2 w}{\partial x^2} - \frac{\partial \gamma_{xz}}{\partial x} \right) \left( 2 \frac{\partial^2 w}{\partial x \partial y} - \frac{\partial \gamma_{xz}}{\partial y} - \frac{\partial \gamma_{yz}}{\partial x} \right) \\ & \left. + 2D_{26} \left( \frac{\partial^2 w}{\partial y^2} - \frac{\partial \gamma_{yz}}{\partial y} \right) \left( 2 \frac{\partial^2 w}{\partial x \partial y} - \frac{\partial \gamma_{xz}}{\partial y} - \frac{\partial \gamma_{yz}}{\partial x} \right) \right] dy dx, \end{aligned} \quad (11)$$

$$U_H = \frac{1}{2} \int_{-a/2}^{a/2} \int_{-b/2}^{b/2} [H_{55} \gamma_{xz}^2 + 2H_{45} \gamma_{xz} \gamma_{yz} + H_{44} \gamma_{yz}^2] dy dx \quad (12)$$

and

$$\begin{aligned} T = & \frac{\lambda}{2} \int_{-a/2}^{a/2} \int_{-b/2}^{b/2} \left[ N_x \left( \frac{\partial w}{\partial x} \right)^2 + N_y \left( \frac{\partial w}{\partial y} \right)^2 \right. \\ & \left. + 2N_{xy} \left( \frac{\partial w}{\partial x} \frac{\partial w}{\partial y} \right) \right] dy dx \end{aligned} \quad (13)$$

respectively, where:  $D_{ij}$  ( $i, j = 1, 2, 6$ ) are the terms of the bending stiffness matrix,  $\mathbf{D}$ ;  $H_{ij}$  ( $i, j = 4, 5$ ) are the terms of the transverse shear stiffness matrix,  $\mathbf{H}$ ;  $w$  is the out-of-plane displacement; and  $\gamma_{xz}$  and  $\gamma_{yz}$  are the transverse shear strains in the  $xz$ - and  $yz$ -directions respectively. The analysis is further simplified and generalised by expressing the total potential energy in the normalised coordinate system of  $\xi$  and  $\eta$  (Equation 7).

### 2.6.2. Shape functions

The shape functions for the out-of-plane displacement and transverse shear strain in the  $xz$ - and  $yz$ -directions are given by:

$$\begin{aligned} w &= \sum_{m=1}^M \sum_{n=1}^N [A_{mn} X_m(\xi) Y_n(\eta)] = A_{mn} X_m Y_n, \\ \gamma_{xz} &= \sum_{f=1}^F \sum_{g=1}^G [D_{fg} F_f(\xi) G_g(\eta)] = D_{fg} F_f G_g, \end{aligned} \quad (14)$$

and

$$\gamma_{yz} = \sum_{k=1}^K \sum_{l=1}^L [E_{kl} K_k(\xi) L_l(\eta)] = E_{kl} K_k L_l,$$

respectively, where: for the  $w$  shape function,  $X_m$  and  $Y_n$  are polynomial series in the  $x$ - and  $y$ -directions respectively,  $M$  and  $N$  are the number of terms in the  $X_m$  and  $Y_n$  series respectively and  $A_{mn}$  are the unknown coefficients; for the  $\gamma_{xz}$  shape function,  $F_f$  and  $G_g$  are polynomial series in the  $x$ - and  $y$ -directions respectively,  $F$  and  $G$  are the number of terms in the  $F_f$  and  $G_g$  series respectively and  $D_{fg}$  are the unknown coefficients; and for the  $\gamma_{yz}$  shape function,  $K_k$  and  $L_l$  are polynomial series in the  $x$ - and  $y$ -directions respectively,  $K$  and  $L$  are the number of terms in the  $K_k$  and  $L_l$  series respectively and  $E_{kl}$  are the unknown coefficients.

A summary of the required shape function boundary conditions for  $w$ ,  $\gamma_{xz}$  and  $\gamma_{yz}$  for given edge boundary conditions are provided in Table 1. The required boundary conditions are implemented through circulation functions applied to the Legendre polynomials [4, 11] in the form:

$$X_i(\xi) = \Gamma_x(\xi) \sum_{i=1}^I L_{i-1}(\xi) \quad \text{where} \quad \Gamma_x(\xi) = (\xi - \xi_c)^n, \quad (15)$$

and the circulation function,  $\Gamma_x(\xi)$ , enforces a condition at  $\xi = \xi_c$  by setting:  $n = 0$  for a free condition;  $n = 1$  for a simply-supported condition ( $X_i = 0$ ); and  $n = 2$  for clamped condition ( $X_i, \partial X_i / \partial \xi = 0$ ).

The total potential energy of the system can then be expressed in terms of the unknowns  $A_{mn}$ ,  $D_{fg}$  and  $E_{kl}$  by substituting the shape functions (Equation 14) into the normalised form of Equations 10-13 and performing numerical integration.

Direction	Description	Boundary condition		
		$w$	$\gamma_{xz}$	$\gamma_{yz}$
$x$ -direction	Simply-supported	S-S	F-F	S-S
	Clamped	C-C	S-S	S-S
$y$ -direction	Simply-supported	S-S	S-S	F-F
	Clamped	C-C	S-S	S-S

Table 1: Boundary conditions and corresponding shape function selection for out-of-plane displacement and transverse shear strains. F: Free ( $n = 0$ ); S: Simply-supported ( $n = 1$ ); C: Clamped ( $n = 2$ ).

### 2.7. Principle of stationary potential energy

Applying the principle of stationary potential energy,  $\delta\Pi = 0$ , to the non-dimensional form of the total potential energy and minimising with respect to the unknown coefficients,  $A_{mn}$ ,  $D_{fg}$  and  $E_{kl}$ , results in a set of linear equations which expressed in matrix form are given by:

$$\left( \begin{bmatrix} \mathbf{K}_{AA} & \mathbf{K}_{AD} & \mathbf{K}_{AE} \\ \mathbf{K}_{AD}^T & \mathbf{K}_{DD} & \mathbf{K}_{DE} \\ \mathbf{K}_{AE}^T & \mathbf{K}_{DE}^T & \mathbf{K}_{EE} \end{bmatrix} - \lambda \begin{bmatrix} \mathbf{L}_{AA} & \mathbf{0} & \mathbf{0} \\ \mathbf{0} & \mathbf{0} & \mathbf{0} \\ \mathbf{0} & \mathbf{0} & \mathbf{0} \end{bmatrix} \right) \begin{bmatrix} \mathbf{A}_{mn} \\ \mathbf{D}_{fg} \\ \mathbf{E}_{kl} \end{bmatrix} = \begin{bmatrix} \mathbf{0} \\ \mathbf{0} \\ \mathbf{0} \end{bmatrix}, \quad (16)$$

where, for example:  $\mathbf{K}_{AD}$  is the stiffness matrix of the  $\mathbf{A}$  coefficients obtained when minimising the strain energy of the system with respect to the  $\mathbf{D}$  coefficient;  $\mathbf{L}_{AA}$  the geometric stiffness matrix; and  $\mathbf{A}_{mn}$ ,  $\mathbf{D}_{fg}$  and  $\mathbf{E}_{kl}$  the vectors of the unknown coefficients.

The solution to the eigenvalue problem of Equation 16 yields stationary points in the total potential energy which are buckling modes of the panel. The eigenvectors provide the coefficients of the out-of-plane displacement and transverse shear strain shape functions, whilst the eigenvalue,  $\lambda$ , the load multiplier of the input uniform end-shortening.

## 3. Parametric study

The parametric study is performed on a long sandwich panel allowing several buckled half-waves to form in the longitudinal direction. As identified by Grdal and co. [1, 18], the performance benefits associated with thin plates with fibre-steering in the lateral direction extend from square plates to long plates, the use of a long panel herein somewhat removes the dependency of lateral edge boundary conditions. The sandwich panel is 1000 mm long, 400 mm wide, with an 8 mm core and 1 mm face-sheets consisting of eight plies of IM7/8552 ( $E_{11} = 161$  MPa,  $E_{22} = 11.38$  MPa,  $G_{12} = 5.17$  MPa,  $\nu_{12} = 0.32$ ,  $t_{\text{ply}} = 0.125$  mm). Whilst the characteristic length to thickness ratio of these panels is relatively high, i.e. 40:1, taking the shorter in-plane dimension which drives the buckling mode shape (refer to Section 2), sandwich panels are typically

Table 2: Core materials and corresponding transverse shear stiffness used in the parametric study [33, 34].

	Core	$G_c$ [MPa]
1	No shear flexibility	$\infty$
2	High density aluminium honeycomb / syntactic foam	1000
3	Medium density aluminium honeycomb	500
4	Low density aluminium honeycomb	200
5	High density aramid honeycomb / low density aluminium honeycomb	100
6	Low density aramid honeycomb	10

used in regions where enhanced structural efficiency, in terms of bending and buckling, is required due to large distances between supported boundaries. Furthermore, transverse shear effects become significant in composite sandwich panels at much lower thickness to characteristic length ratios than monolithic composites due to the high ratio of in-plane stiffness to transverse shear stiffness present in sandwich panels [5].

The critical buckling load was determined for the case of uniform end-shortening with longitudinal edges free to expand and all edges simply-supported. The VS skin is achieved with a linear variation in the  $y$ -direction symmetric about the centre line of the panel ( $y=0$ ) in the form  $[\pm\langle T_1|T_2\rangle_2]_s$ , where  $T_1$  and  $T_2$  are located at the edge and centre line of the panel, i.e.  $y_1=b/2$  and  $y_2=0$  respectively, as shown in Figure 1. Six different isotropic core properties were considered as detailed in Table 2, all representing practical values ranging from high density aluminium honeycomb, or syntactic foam, to low density aramid honeycomb [33, 34].

It should be noted, that sandwich panels can fail through a variety of mechanisms including: material strength of either the face-sheets or core; and various instabilities such as intra-cell dimpling, face wrinkling, shear crimping, and global buckling. The focus of this study, however, is on global instabilities present when idealising the structure as a thick two-dimensional plate, i.e. global buckling and shear crimping. Strength based failure modes, as well as intra-cell dimpling and face wrinkling, are not captured or discussed further.

To enable observation of the qualitative effect of the core's shear stiffness, the core's contribution to axial and bending stiffnesses of the panel is neglected. For sandwich panels, the overall in-plane and flexural stiffnesses are often dominated by skin properties alone and in-plane properties of the core, such as Poisson's ratio and Young's modulus, do not affect buckling behaviour or loads to any great extent.

For VS structures, it is convenient to present the stiffness and buckling loads as smeared (or averaged) values due to their non-uniformity, which for the pre-buckling stiffness and critical buckling load are given

by:

$$E_{x,\text{sm}} = \frac{a}{bh\Delta x} \int_{-b/2}^{b/2} \left[ N_x(y)|_{x=-a/2} \right] dy, \quad (17)$$

and

$$N_{x,\text{sm}} = \frac{1}{b} \int_{-b/2}^{b/2} \left[ N_x(y)|_{x=-a/2} \right] dy, \quad (18)$$

respectively. The pre-buckling stiffness and critical buckling load were obtained for every combination of angle for  $T_1$  and  $T_2$  varying from  $0^\circ$  to  $90^\circ$  in  $5^\circ$  increments for all core values provided in Table 2. However, as an introduction to the form of plots used to present the results, and to serve as a baseline comparison, results are first provided for the case of a thin 2 mm plate neglecting transverse shear effects ( $[\pm\langle T_1|T_2 \rangle_2]_{2s}$ ). The normalised smeared critical buckling load is plotted against the normalised smeared pre-buckling stiffness, given by:

$$\hat{N}_{x,\text{sm}} = \frac{N_{x,\text{sm}}}{\max [N_{x,\text{sm}}|_{T_1=T_2}]} \quad \text{and} \quad \hat{E}_{x,\text{sm}} = \frac{E_{x,\text{sm}}}{\max [E_{x,\text{sm}}]}, \quad (19)$$

respectively, in Figure 2. Here, the buckling load is normalised against the maximum straight-fibre configuration buckling load and can be considered a VS factor of improvement, whilst the pre-buckling stiffness is normalised against the maximum pre-buckling stiffness, which occurs for an all  $0^\circ$  straight-fibre laminate.

The data is plotted in sets of  $T_2$  angles with an additional plot for straight-fibre configurations ( $T_1=T_2$ ). This form of plot was first used to illustrate the design space of VS laminates for buckling by Olmedo and Gürdal [1]. The thick dashed line is the straight-fibre configuration and the thin black lines VS which are labelled in  $15^\circ$  increments for  $T_2$  in Figure 2. The area bound by the VS curves represents a significant increase in design space when compared to the straight-fibre configurations. The maximum buckling load achieved with VS occurs for a  $\langle 15^\circ|80^\circ \rangle$  variation and is 64% higher than the maximum straight-fibre buckling load which occurs at an angle of  $\pm 45^\circ$ .

The results obtained for the various transverse shear moduli sandwich panel configurations, including transverse shear effects, are provided in Figure 3. Panels neglecting core shear flexibility ( $G_c = \infty$  MPa) or with high core transverse shear stiffness ( $G_c = 1000, 500$  MPa) showed similar buckling characteristics and relative improvements over straight-fibre configurations as the thin VS plates of the same aspect ratio provided in Figure 2, having approximately a peak improvement of 62% for a  $\langle 15^\circ|85^\circ \rangle$  fibre path. However, further decreasing the core shear modulus to 200 MPa resulted in the normalised buckling plots in Figure 3 taking a different form, with an associated reduction in improvements of VS panels when compared to straight-fibre configurations; the behaviour becoming more prevalent with further reductions in core transverse shear modulus.

The change in behaviour and loss of performance displayed in Figure 3 for panels with low shear modulus cores are attributed to the critical buckling mode of the panel changing from global to core shear crimping,

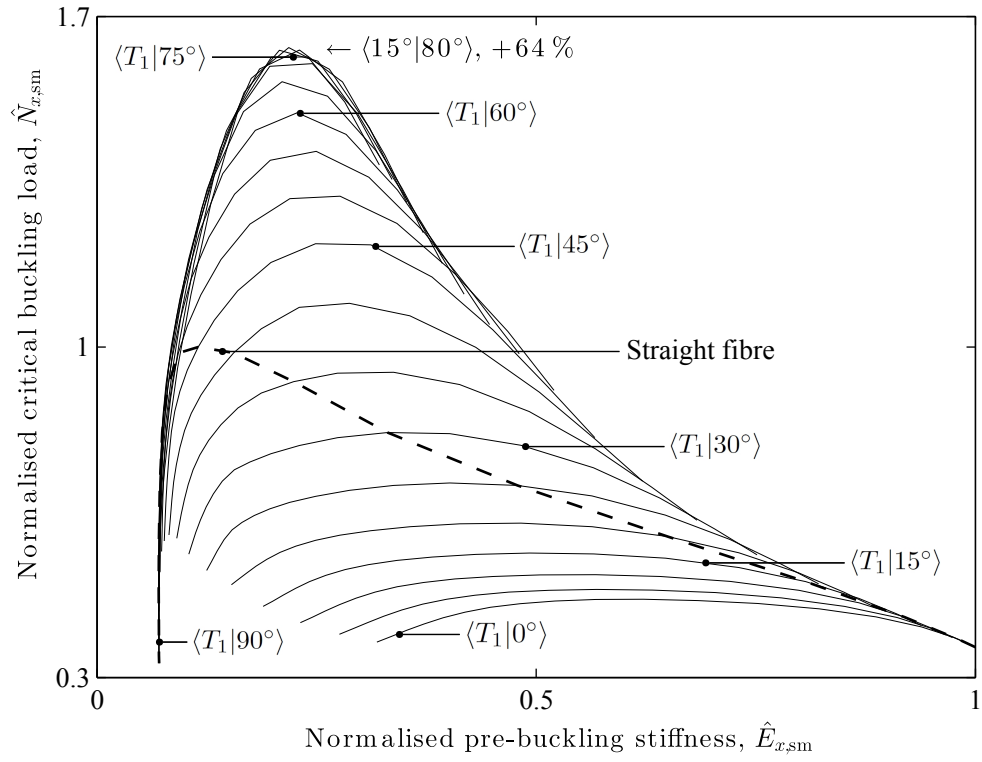
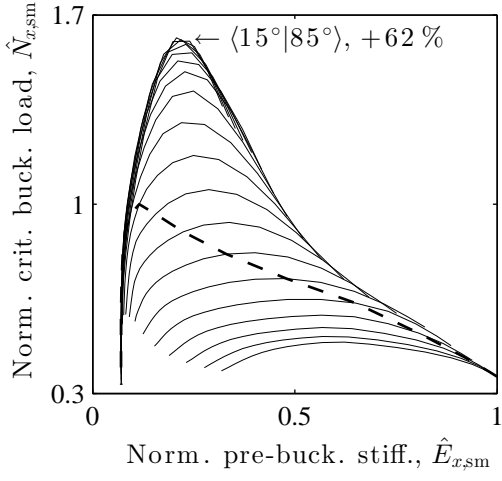
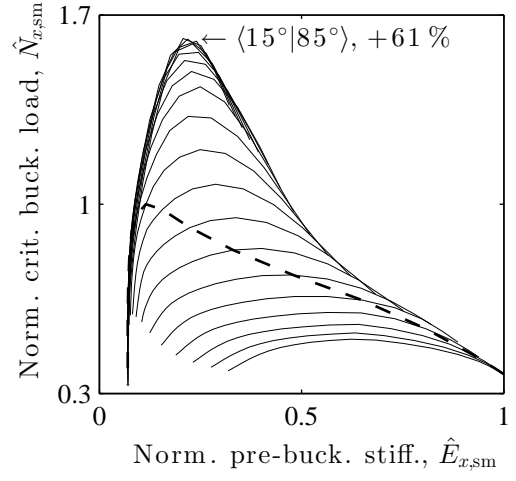


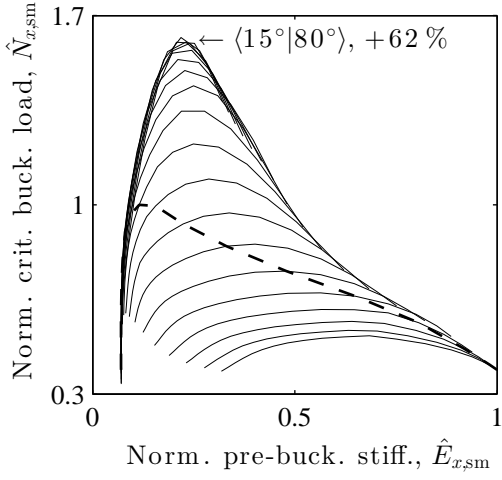
Figure 2: Normalised smeared critical buckling load against normalised smeared pre-buckling stiffness for a thin monolithic plate with a linear fibre variation in the  $y$ -direction.



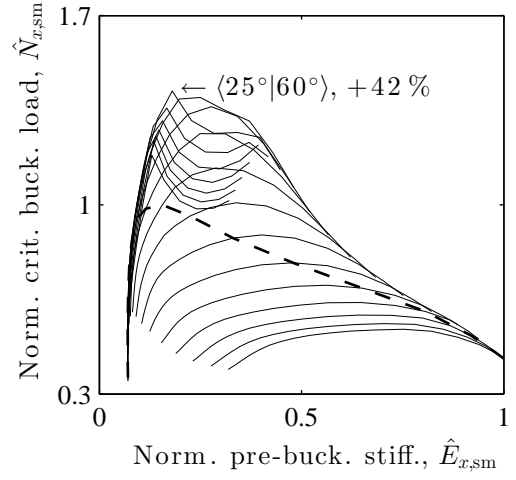
(a) Core 1,  $G_c = \infty$ .



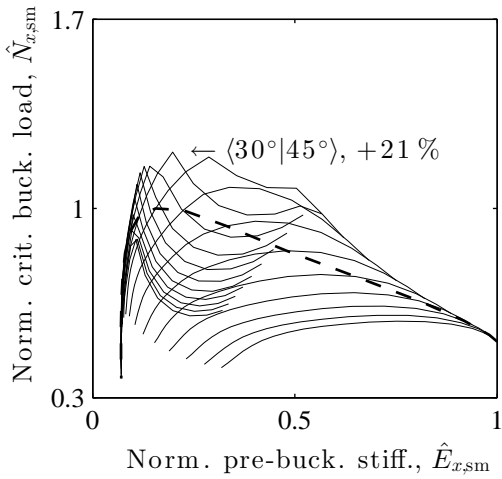
(b) Core 2,  $G_c = 1000$  MPa.



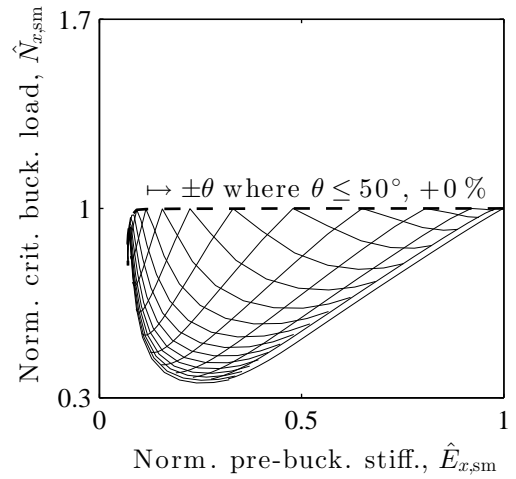
(c) Core 3,  $G_c = 500$  MPa.



(d) Core 4,  $G_c = 200$  MPa.



(e) Core 5,  $G_c = 100$  MPa.



(f) Core 6,  $G_c = 10$  MPa.

Figure 3: Normalised smeared critical buckling load against normalised smeared pre-buckling stiffness for various sandwich core shear moduli. Thin continuous lines are for fixed central angle,  $T_2$  with variable  $T_1$ , and dashed lines indicate straight-fibre configurations ( $T_1 = T_2$ ).



Figure 4: One-dimensional sandwich panel buckling modes.

as shown in Figures 4a and Figure 4b respectively for a one-dimensional case. This can be best explained by examining a single curve; the profile for core five ( $G_c = 100$  MPa) with VS  $[\pm \langle T_1 | 45^\circ \rangle_2]_s$  skins ( $T_2$  fixed at  $45^\circ$ ) obtained by varying  $T_1$  from  $0^\circ$  to  $90^\circ$  in  $5^\circ$  increments is provided in Figure 5b, showing both global and shear crimping buckling loads. With increasing pre-buckling stiffness, by varying  $T_1$  from  $90^\circ$  towards  $0^\circ$ , the buckling load of the panel initially increases with critical modes being global, occurring over the full width of the panel with two to five half-waves in the  $x$ -direction. This increase in critical buckling load continues until a maximum absolute critical buckling load of  $0.710$  kN/mm at a fibre path of  $\langle 30^\circ | 45^\circ \rangle$  is reached, 21 % higher than the best straight-fibre configuration. Further decreasing  $T_1$  beyond  $30^\circ$  results in an abrupt decrease in critical buckling load accompanied by a change in the buckling mode to shear crimping occurring in localised regions towards boundary supports. Shear crimping modes continue to occur with decreasing  $T_1$  until a configuration of  $\langle 10^\circ | 45^\circ \rangle$  at which global modes again become critical.

Core shear crimping instabilities are short wavelength buckling modes in which displacements are predominately due to transverse shearing, rather than rotation, and are attributed to a low core shear modulus. The *local* load at which crimping occurs is almost independent of skin properties and for a uniaxially loaded sandwich panel with straight-fibre face-sheets, the critical shear crimping load is given by Vinson [35] as:

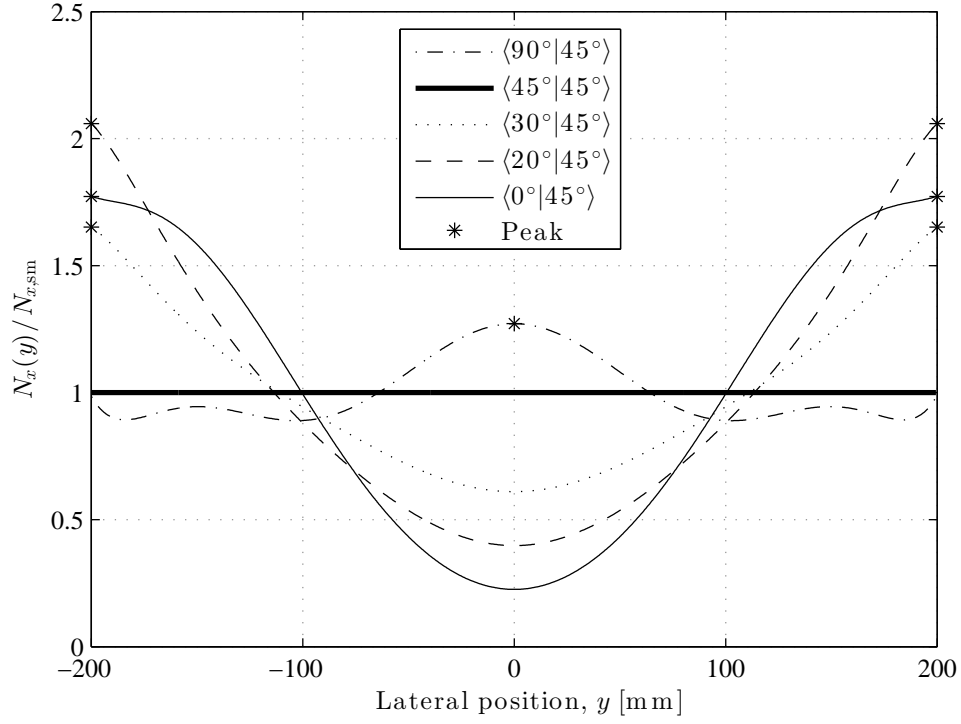
$$N_{\text{crimp}} = G_c h_c. \quad (20)$$

Equation 20 is applicable to sufficiently long and wide panels such that the short-wavelength crimping mode is unaffected by boundary conditions. In the derivation, Vinson [35] additionally assumed very thin face-sheets, i.e. the depth of the core can be equated to the distance between the midplane of the face-sheets, when determining the equivalent transverse shear rigidity, and thus Equation 20 can provide underestimations for face-sheets of practical thicknesses. An improvement to Equation 20 is to assume only thin face-sheets, i.e. the depth of the core cannot be equated to the distance between the midplane of the face-sheets, and use an equivalent core thickness for determining the transverse shear rigidity as applied in Equation 3, i.e.

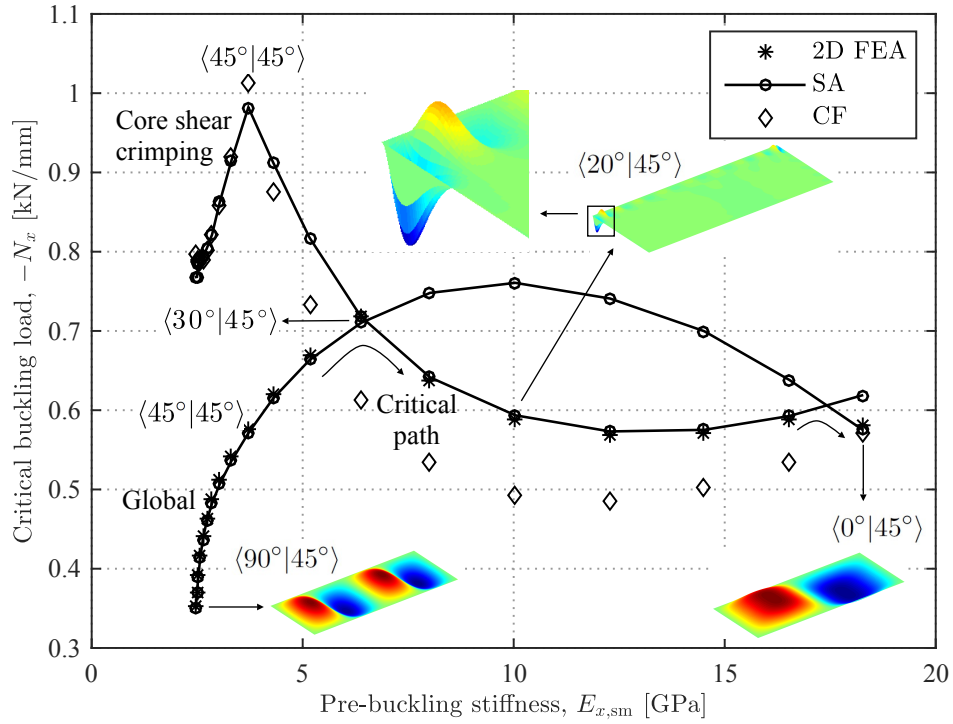
$$N_{\text{crimp}} = G_c h_e \quad \text{where} \quad h_e = \frac{(h_{\text{fs}} + h_c)^2}{h_c}. \quad (21)$$

Equation 21 provides an increase in the panel's transverse shear rigidity and consequently its critical shear crimping loads. In the case of very thin face-sheets, Equations 20 and 21 yield the same results, however for all panels considered in this chapter ( $h_c = 8$  mm,  $h_{\text{fs}} = 1$  mm) the shear rigidity of the modified approach,





(a) Semi-analytical ( $H = 10$ ) normalised pre-buckling in-plane stress resultant,  $N_x$ ,  $y$ -direction distribution when subject to a uniform end-shortening. \* indicates the lateral location of peak in-plane stress resultants for VS face-sheets and consequently the lateral location of the local shear crimping instability.



(b) Smeared critical buckling load plotted for two-dimensional FEA (2D FEA), semi-analytical model (SA), and closed-form (CF) solution as per Equation 22. FEA results provided for critical path only, and CF for shear crimping modes only.

Figure 5: Low shear modulus core five,  $G_c = 100$  MPa, with a  $\langle T_1 | 45^\circ \rangle$  VS skin.

Equation 21, is 27 % larger than Equation 20.

Being short in wavelength, shear crimping instabilities are able to occur in localised regions. In the pre-buckled state, the VS load redistribution, as shown in Figure 5a, creates highly loaded regions which locally exceed the critical shear crimping load, being primarily a function of core properties alone (Equation 21). This is shown by the  $\langle 20^\circ | 45^\circ \rangle$  mode in Figure 5b, where shear crimping occurs in a strip at the location of the highly loaded  $20^\circ$  fibre angles with the remainder of the panel, being below the shear crimping load, remaining unbuckled. Likewise, the  $\langle 90^\circ | 45^\circ \rangle$ , with a  $90^\circ$  orientation at boundaries and  $45^\circ$  at the centre, has a shear crimping mode occurring in the, relatively, highly loaded central region. The maximum shear crimping buckling load in Figure 5b is achieved when the panel is loaded with a uniform stress with the straight-fibre configuration of  $\langle 45^\circ | 45^\circ \rangle$ . Here, the entire width of the panel is able to fail simultaneously in shear crimping rather than in a local region.

The critical shear crimping loads provided in Equations 20 and 21 are strictly only valid for straight-fibre face-sheet sandwich panels, however, can be used for qualitative purposes to predict the onset of local shear crimping in VS sandwich panels due to the short-wavelength of the modes. Applying this hypothesis, the smeared, or panel level, critical buckling load at which this occurs can then be given by:

$$N_{\text{sm,crimp}} = \underbrace{G_c h_e}_{\text{Core}} \times \underbrace{\frac{E_{x,\text{sm}}}{E_{x,\text{peak}}}}_{\text{VS face-sheet}} \quad (22)$$

where  $E_{x,\text{peak}}$  is the peak in-plane stiffness across the width of the panel, for the case of the longitudinal edges being free to expand. The first component of Equation 22,  $G_c h_e$ , can be considered the panel's transverse shear rigidity, or resistance to shear crimping, whilst the second component,  $E_{x,\text{sm}}/E_{x,\text{peak}}$ , a measure of load redistribution due to VS, which is unity for straight-fibre panels and less than unity for VS panels, effectively reducing the panel's smeared critical shear crimping load. These two components are almost completely decoupled into core properties ( $G_c h_e$ ) and VS face-sheet properties ( $E_{x,\text{sm}}/E_{x,\text{peak}}$ ), and thus both the core and VS face-sheets independently influence, through different mechanisms, the panel level smeared shear crimping load. It should be noted, that whilst Equation 22 is closed-form, it requires determination of the smeared and peak in-plane stiffnesses of the panel.

The critical shear crimping load determined with Equation 22 is additionally plotted for the  $G_c = 100 \text{ MPa}$   $\langle T_1 | 45^\circ \rangle$  panels in Figure 5b. Crimping loads obtained with the closed-form solution provide a good estimate for the cases where the peak stiffness, and consequently crimping failure, is in the centre of the panel, e.g.  $\langle 90^\circ | 45^\circ \rangle$ , or where there is a uniform distribution, i.e.  $\langle 45^\circ | 45^\circ \rangle$ . For peak stiffnesses located at the panel boundaries, i.e.  $T_1 < 45^\circ$ , the simply-supported conditions provide a stiffening effect not captured with the closed-form solution, and hence Equation 22 under-predicts when compared to the semi-analytical model and FEA. Nonetheless, Equation 22 is able to qualitatively describe the shear crimping behaviour of VS sandwich panels.

Returning focus back to Figure 3, for core six (Figure 3f) with a core shear modulus of 10 MPa, even the slightest load variation results in local shear crimping and thus the optimal VS configurations coincide with the straight-fibre laminates. For angles greater than  $50^\circ$  the straight-fibre configurations for core six buckle in global modes and plateau at a constant maximum below this angle in shear crimping, as per Equation 21.

In all results presented, the semi-analytical model used 10 terms in the pre-buckling analysis whilst for the buckling analysis a different amount of terms were used for high and low shear modulus cores, due to the high frequency waves that occurred with shear crimping. For high shear modulus cores (cores one to three) 15 and 9 terms (405 degrees of freedom) were used in the  $x$ - and  $y$ -directions respectively, whilst for low modulus cores (cores four to six) 20 and 15 terms (900 degrees of freedom) were used in the  $x$ - and  $y$ -directions respectively.

Critical buckling loads were additionally computed with ABAQUS 6.12-1 [36] for specific panels using, firstly, two-dimensional shell elements (Figure 5b), and secondly, three-dimensional solid elements (Figure 6), both idealisations employing a linear buckling analysis. The VS was achieved in the FEA by rotating the local element material coordinate system, i.e. fixed fibre angle per element. Core material properties of  $E_{11} = E_{22} = 6$  MPa,  $E_{33} = 600$  MPa,  $G_{12} = 1$  MPa,  $G_{13} = G_{23} = 100$  MPa,  $\nu_{12} = 0.25$ ,  $\nu_{13} = \nu_{23} = 0.0025$  were assumed.

Two-dimensional FE results were obtained for uniaxially loaded and simply-supported VS  $[\pm(T_1|45^\circ)_2]_s$  sandwich panels as per Figure 5b. The FE model achieved converged results with 4000 10 mm square S4R quadrilateral shell elements ( $20 \times 10^3$  degrees of freedom). The FSDT employed in S4R shell elements for ABAQUS establishes an equivalent shear factor for the sandwich panel by equating the shear strain energy of the accurate distribution (assuming piecewise parabolic distributions in each layer) to the strain energy with the assumed profile (constant for FSDT) [36]. Results obtained with the two-dimensional FE model are therefore considered to be more accurate in terms of transverse shear deformation than the semi-analytical model. The same boundary conditions that were applied to the semi-analytical model were also applied to the two-dimensional FE model. Semi-analytical results presented in Figure 5b were within 1 % of the two-dimensional FEA and required over an order of magnitude less degrees of freedom. An advantage of using polynomials as the semi-analytical shape functions is their ability to allow regions to exhibit short wavelength modes *locally*, capturing the shear crimping failure modes as shown in Figure 5b.

Comparison of the semi-analytical model with three-dimensional FE was performed on the same configuration as per the two-dimensional case that is shown in Figure 5b, with the exception of applying clamped boundary conditions along all edges instead of simply-supported. The use of clamped boundary conditions was required due to the difficulty in implementation of simply-supported boundary conditions in a three-dimensional structure in terms of load introduction and buckling mode shapes. Clamped boundary conditions were achieved by constraining all loaded faces to remain flat (null rotation in all directions), with only the geometric midplane of the sandwich panel constrained in out-of-plane displacement, i.e. the

$xy$ -planform	Mesh density			$-N_{x,sm,crit}$	
	Face-sheet ply	Core	Elms	[kN/mm]	Error
10 mm	1 elm. (0.125 mm)	2 elm. (4 mm)	$72 \times 10^3$	0.8485	1.48 %
5 mm	1 elm. (0.125 mm)	2 elm. (4 mm)	$288 \times 10^3$	0.8375	0.16 %
5 mm	1 elm. (0.125 mm)	8 elm. (1 mm)	$384 \times 10^3$	0.8367	0.07 %
5 mm	3 elm. (0.042 mm)	6 elm. (1.33 mm)	$864 \times 10^3$	0.8361	-

Table 3: Three-dimensional FE convergence study for  $G_c = 100$  MPa with a  $\langle 20|45^\circ \rangle$  VS skin, subject to uniaxial loading with all edges clamped. The critical mode was shear crimping in all cases. Percentage error is relative to the highest mesh density configuration.

loaded edges were free to expand in the  $z$ -direction about the midplane. The mesh consisted of  $288 \times 10^3$  C3D8R linear hexahedron solid elements ( $928 \times 10^3$  degrees of freedom). Element lengths in the plane of the structure ( $x$ - and  $y$ -directions) were 5 mm whilst through the depth of the structure ( $z$ -direction) one element per face-sheet ply (0.125 mm depth) and two elements (4 mm depth) for the core were used. This mesh density was found to achieve converged results, with increases in the number of elements through the thickness of the structure by a factor of three providing less than 0.2 % improvement in shear crimping buckling loads as detailed in Table 3.

The results for the three-dimensional FE and semi-analytical model are provided in Figure 6. Three-dimensional FE results are in good agreement with the semi-analytical for global modes, lying within 5 % of each other, however, for shear crimping modes this error increases to 13 %. As discussed in Section 2, the characteristic length to thickness ratio, which can be used as a rule-of-thumb guide to the importance of through thickness behaviour, is strictly dependent on the dimension of the buckling wavelength. For all global modes presented in Figure 6, three to four half-waves occurred in the longitudinal direction, and one in the transverse direction, with the small dimension of the half-waves ranging from approximately 250 mm ( $1000 \text{ mm}/4$ ) to 333 mm ( $1000 \text{ mm}/3$ ), corresponding to characteristic length to thickness ratios of 25:1 (250 mm:10 mm) and 33:1 (333 mm:10 mm). For the shear crimping modes presented in Figure 6, the size of the half-waves can be qualitatively estimated to be less than 100 mm, i.e. one quarter of the panels width, resulting in a characteristic length to thickness ratio as low as 10:1 (100 mm:10 mm). Owing to the high frequency mode shapes, and thus low characteristic length to thickness ratio, the shear crimping modes are influenced to a greater extent than the large wavelength global modes with the increased modelling of through thickness stresses and deformations. Nonetheless, at ratios of 10:1 through thickness stresses are expected to be significant, and thus agreement within 13 % of three-dimensional FEA, considering the simplicity of the FSDT, suggest a good correlation. Furthermore, the semi-analytical model required over three orders of magnitude less degrees of freedom than the three-dimensional FE and similar trends are

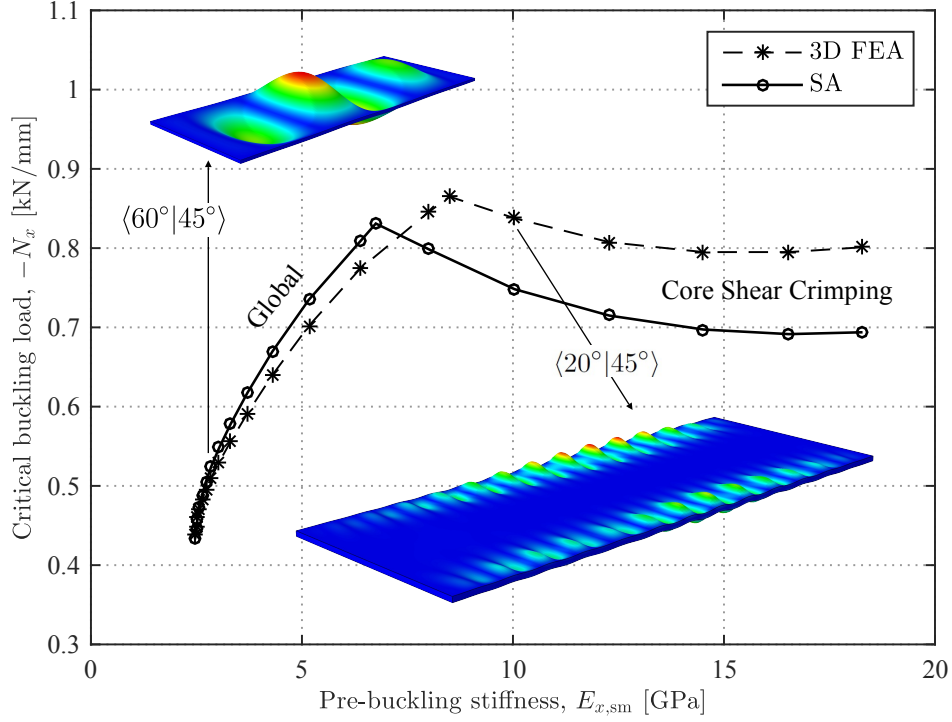


Figure 6: Smeared critical buckling load plotted for three-dimensional FEA (3D FEA) and semi-analytical model (SA).  $G_c = 100$  MPa, with a  $\langle T_1 | 45^\circ \rangle$  VS skin, all edges clamped, uniaxial loading. Buckling mode shapes shown are for three-dimensional FE, with colours indicating displacement magnitude. Intersection point between modes was not computed and is added for illustrative purposes only.

observed for both data sets, thus validating the use of the FSDT for qualitative purposes and use in design.

#### 4. Optimisation

Using the same panel configuration as the parametric study an optimisation study was performed for all six core cases with an increasing amount of control points enabling increased tailorability of the fibre path. The optimisation procedure, implemented in MATLAB R2013a [27], consisted of a hybrid approach; an initial genetic algorithm (GA), followed by a interior-point algorithm starting from the GA's solution. This approach utilises the enhanced global performance of GAs to identify a near-optimum solution and then switches to a faster and more efficient method for local searching. Owing to the small number of variables in the optimisation problem, ranging from one to four, confidence with the procedure, i.e. convergence to the global optimum, was able to be achieved without the use of large, and computationally expensive, population sizes or number of generations. For each core, the optimum was found with variations using evenly spaced control points symmetric about  $y = 0$ ; one control point  $[\pm T_1]_{2s}$  (straight-fibre configuration); two control

Table 4: VS sandwich panel optimisation study results. Buckling loads are expressed as smeared stress resultants,  $-N_{x,sm,crit}$  [kN/mm], and optimal fibre angles rounded to the nearest integer value. Number in brackets is percentage improvement relative to optimal straight-fibre (single control point) buckling load. CP: control points.

$G_c$	$[\pm\langle T_1^\circ \rangle_2]_s$		$[\pm\langle T_1^\circ   T_2^\circ \rangle_2]_s$		$[\pm\langle T_1^\circ   T_2^\circ   T_3^\circ \rangle_2]_s$		$[\pm\langle T_1^\circ   T_2^\circ   T_3^\circ   T_4^\circ \rangle_2]_s$	
[MPa]	CP	$-N_{x,sm,crit}$	CP	$-N_{x,sm,crit}$	CP	$-N_{x,sm,crit}$	CP	$-N_{x,sm,crit}$
$\infty$	44°	0.90	13° 90°	1.46 (61.6 %)	8° 62° 56°	1.56 (73.4 %)	1° 53° 57° 60°	1.56 (78.4 %)
1000	43°	0.86	13° 86°	1.39 (61.2 %)	7° 62° 56°	1.50 (73.7 %)	1° 53° 56° 59°	1.54 (78.5 %)
500	42°	0.82	14° 82°	1.31 (60.5 %)	8° 61° 54°	1.42 (73.9 %)	1° 52° 55° 57°	1.46 (78.5 %)
200	39°	0.71	24° 57°	1.01 (42.7 %)	24° 40° 60°	1.02 (42.7 %)	24° 32° 53° 50°	1.03 (44.2 %)
100	39°	0.59	31° 46°	0.71 (21.1 %)	31° 35° 53°	0.72 (22.6 %)	32° 33° 42° 49°	0.72 (22.7 %)
10	13°	0.10	4°  6°	0.10 ( 0.2 %)	4°  8°  7°	0.10 ( 0.3 %)	2°  9°  7°  9°	0.10 ( 0.4 %)

points  $[\pm\langle T_1 | T_2 \rangle_2]_s$  at  $y=[0.50b, 0.00]$ ; three control points  $[\pm\langle T_1 | T_2 | T_3 \rangle_2]_s$  at  $y=[0.50b, 0.25b, 0.00]$ ; and four control points  $[\pm\langle T_1 | T_2 | T_3 | T_4 \rangle_2]_s$  at  $y=[0.50b, 0.33b, 0.17b, 0.00]$ . A summary of the optimisation results are provided in Table 4.

Optimised solutions for one and two control points typically identified configurations very close to the parametric study results, with absolute critical buckling loads only improving by up to 2.4 %, hence validating the usefulness of the coarse parametric plots, particularly when considering the additional insight provided. **Cores with a high shear modulus ( $G_c = \infty, 1000, 500$  MPa) failed with global buckling as the critical mode for all optimised configurations. In this case,** increasing the number of control points resulted in an improvement in buckling load, albeit to a lesser extent with each refinement, plateauing just under 80 % improvement with four control points. The optimal configurations tended to distribute load towards boundaries and reduce loading in a large central region of the panel using an almost constant fibre angle with low axial stiffness as shown in Figure 7a. For example, the optimal four control point fibre path of the 500 MPa core was  $[\pm\langle 1^\circ | 52^\circ | 55^\circ | 57^\circ \rangle_2]_s$ . With increasing control points, the solutions appeared to approach a configuration creating highly loaded axial beams along the boundaries connected by a shear web. Such configurations, however, require fibres to be steered with large in-plane fibre curvatures towards boundaries and thus manufacturability may be an issue. This configuration is optimising with global buckling as the driver, with the high shear modulus core alleviating crimping as a critical mode as per Equation 22.

**The optimal configuration of cores with a low shear modulus ( $G_c = 200, 100, 10$  MPa) occurred when global and shear crimping modes were approximately equal to each other, as can be seen by the parametric plots in Figure 3, thus representing the peak in buckling performance. These configurations** additionally had optimal fibre paths leading to increased loading towards boundaries for enhanced global buckling performance. Here, the amount of redistribution, or more specifically the ratio smeared to peak in-plane stiffness

$(E_{x,\text{sm}}/E_{x,\text{peak}})$ , was limited due to crimping modes occurring. For example, the optimal four control point fibre path of the 200 MPa core was  $[\pm(24^\circ|32^\circ|53^\circ|50^\circ)_2]_s$  as shown in Figure 7b. These cores tended to reach an upper limit in improvement over straight-fibre configurations at only two control points; with this simple linear variation seemingly a close approximation of optimal fibre paths with additional control points. The core with a shear modulus of 10 MPa found little improvement with any fibre steering due to the minimal core shear flexibility; promoting local shear crimping in the presence of minor load redistributions.

It should be noted, that whilst the linear buckling analysis predicts the onset of a single buckling mode, being either global or shear crimping, mode interaction in the post-buckling regime may occur directly after the initial buckling event. In the case of the critical mode being global, shear crimping or localised face-sheet buckling [37] (not captured with the presented two-dimensional model) can occur. Here, the transverse shear stresses in the core or in-plane stresses in the skin that occur in global modes can potentially promote shear crimping or localised face-sheet buckling respectively. Similarly, if shear crimping is the critical mode, the panel has a reduced axial load carrying capability in the region of the buckle and thus the flexural rigidity is additionally reduced which may lead to global buckling. Experimentally, difficulty would be expected in ascertaining which buckling mode was critical as failure may occur simultaneously, particularly if the linearly predicted buckling modes occur at similar loads. From a design point of view, however, the prediction of linear buckling loads for the different modes remains of importance to allow design measures to prevent each mode occurring and provide physical insight into the structural behaviour.

## 5. Conclusion

In this paper, the benefits of VS sandwich panels for enhanced buckling performance were explored by allowing face-sheet laminates to have steered fibres in the lateral direction ( $y$ -direction). A semi-analytical Ritz model was first developed performing a pre-buckling analysis using the total complementary energy to determine the non-uniform stress resultants, followed by a linear buckling analysis, including a FSDT, on the total potential energy to determine buckling loads and mode shapes. Including a FSDT, the model is able to capture both bending dominated global buckling modes, characterised by large wavelengths, and transverse shear dominated crimping instabilities, characterised by short wavelengths.

The developed model was subsequently used in a parametric study on long uniaxially loaded and simply-supported sandwich panels, varying both the fibre angle path along the lateral direction and core shear modulus. Results revealed that shear crimping can occur at a significantly reduced load in VS sandwich panels compared to their straight-fibre counterparts. For low shear modulus cores, these modes were found to become critical, reducing the relative buckling performance of VS sandwich panels when compared to straight-fibre configurations. For the cases considered, cores with a shear modulus of at least 500 MPa experienced global buckling as the critical mode, with optimal VS configurations having approximately

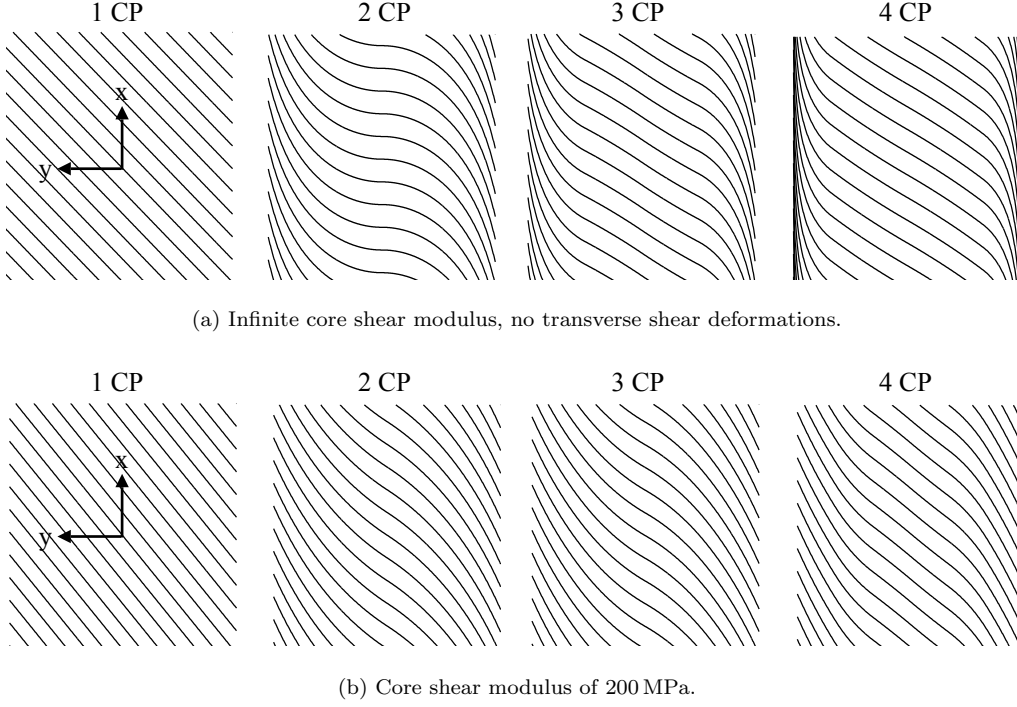


Figure 7: Optimised face-sheet fibre paths for 1, 2, 3 and 4 control points (CP) variations.

a 60 % higher critical buckling load than straight-fibre panels. Here, the mechanism of improvement and optimal fibre angle variation were similar to that of thin plates, steering from approximately  $80^\circ$  at the centre of the plate to  $15^\circ$  at boundaries to redistribute in-plane loads to the supported edges. The promotion of the crimping modes in VS sandwich panels with low shear modulus cores is due to the pre-buckling load redistribution creating local regions with peak in-plane stresses, significantly higher than the smeared (average) in-plane stress of the panel, which *locally* exceed the critical shear crimping load and trigger the short wavelength mode. The smeared load at which shear crimping occurs was found to be directly and inversely proportional to the panel's transverse shear rigidity (largely due to core properties) and the extent of load redistribution (the ratio of peak to smeared in-plane stiffness, a VS face-sheet property) respectively. Thus a straight-fibre panel, having no load redistribution, represents the best configuration for shear crimping performance.

Semi-analytical results for specific cases were compared against both two- and three-dimensional FEA, critical buckling loads were found to be within 1 % and 13 % whilst requiring approximately one and three orders of magnitude less degrees of freedom respectively. Furthermore, similar trends were observed for all data sets, thus validating the use of the FSDT for qualitative purpose and use in design. Future work could include the application of more advanced plate models that capture the effect of highly inhomogeneous material properties more accurately.



Applying the same loading, boundary conditions and geometry as the parametric study, an optimisation study was performed on the sandwich panels with various core properties utilising up to a four control point fibre variation. Optimised configurations of high modulus cores ( $G_c \geq 500$  MPa) had improvements in critical buckling loads, over straight-fibre panels, of 78 % with four control points. Here, the optimal fibre paths tended to increase pre-buckling loading towards the boundaries, with angles close to  $0^\circ$ , and rapidly reduce loading in a large central region with an almost constant fibre angle. Cores with low shear moduli ( $G_c < 500$  MPa), on the other hand, tended to utilise a less aggressive load redistribution, to prevent premature shear crimping at a low panel level load, and had reduced improvements in critical buckling load relative to straight-fibre panels. With reducing core shear modulus, the improvement decreased from 78 % ( $G_c \geq 500$  MPa) to less than 1 % for a 10 MPa shear modulus core.

The transverse shear flexibility and load redistribution are two key parameters that must be considered carefully in the design of sandwich panels to exploit the benefits of VS fully in this novel structural configuration.

## Acknowledgements

The authors gratefully acknowledge the support of the EPSRC under its ACCIS Centre for Doctoral Training Grant, EP/G036772/1.

## References

- [1] R. Olmedo and Z. Gürdal, “Buckling response of laminates with spatially varying fiber orientations,” in *34th Structures, Structural Dynamics, and Materials Conference*, no. AIAA-93-1567-CP, (La Jolla, CA, U.S.A.), AIAA, 1993.
- [2] P. M. Weaver, K. D. Potter, K. Hazra, M. A. R. Saverymuthapulle, and M. T. Hawthorne, “Buckling of variable angle tow plates: from concept to experiment,” in *50th AIAA/ASME/ASCE/AHS/ASC Structures, Structural Dynamics, and Materials Conference*, no. AIAA-2009-2509, (Palm Springs, CA, U.S.A.), AIAA, 2009.
- [3] S. T. IJsselmuiden, M. M. Abdalla, and Z. Gürdal, “Optimization of variable-stiffness panels for maximum buckling load using lamination parameters,” *AIAA Journal*, vol. 48, no. 1, pp. 134–143, 2010.
- [4] Z. Wu, P. M. Weaver, G. Raju, and B. Chul Kim, “Buckling analysis and optimisation of variable angle tow composite plates,” *Thin-Walled Structures*, vol. 60, pp. 163–172, 2012.
- [5] R. Groh, P. M. Weaver, S. C. White, G. Raju, and Z. Wu, “A 2D equivalent single-layer formulation for the effect of transverse shear on laminated plates with curvilinear fibres,” *Composite Structures*, vol. 100, pp. 464–478, 2013.
- [6] Z. Wu, G. Raju, and P. M. Weaver, “Postbuckling analysis of variable angle tow composite plates,” *International Journal of Solids and Structures*, vol. 50, no. 10, pp. 1770–1780, 2013.
- [7] G. Raju, Z. Wu, and P. M. Weaver, “Buckling and postbuckling of variable angle tow composite plates under in-plane shear loading,” *International Journal of Solids and Structures*, vol. 58, pp. 270–287, 2015.
- [8] S. C. White, G. Raju, and P. M. Weaver, “Initial post-buckling of variable-stiffness curved panels,” *Journal of the Mechanics and Physics of Solids*, vol. 71, pp. 132–155, 2014.
- [9] B. H. Coburn, Z. Wu, and P. M. Weaver, “Buckling analysis of stiffened variable angle tow panels,” *Composite Structures*, vol. 111, pp. 259–270, 2014.

- [10] B. H. Coburn, Z. Wu, and P. M. Weaver, "Local buckling of blade stiffened variable angle tow panels," in *AIAA/ASME/ASCE/AHS/ASC 55th Structures, Structural Dynamics, and Materials Conference*, no. AIAA 2014-0167, (Washington, D.C., U.S.A), AIAA, 2014.
- [11] B. H. Coburn and P. M. Weaver, "Buckling analysis and optimization of blade stiffened variable stiffness panels," in *AIAA/ASME/ASCE/AHS/ASC 56th Structures, Structural Dynamics, and Materials Conference*, no. AIAA 2015-1438, (Kissimmee, FL, U.S.A.), AIAA, 2015.
- [12] M. W. Hyer and H. Lee, "The use of curvilinear fiber format to improve buckling resistance of composite plates with central circular holes," *Composite Structures*, vol. 18, no. 3, pp. 239–261, 1991.
- [13] A. Khani, S. T. IJsselmuiden, M. Abdalla, and Z. Gürdal, "Design of variable stiffness panels for maximum strength using lamination parameters," *Composites Part B: Engineering*, vol. 42, no. 3, pp. 546–552, 2011.
- [14] K. C. Wu, B. F. Tatting, and B. Smith, "Design and manufacturing of tow-steered composite shells using fiber placement," in *50th AIAA/ASME/ASCE/AHS/ASC Structures, Structural Dynamics, and Materials Conference*, no. AIAA-2009-2700, (Palm Springs, CA, U.S.A.), AIAA, 2009.
- [15] A. S. Panesar, K. Hazra, and P. M. Weaver, "Investigation of thermally induced bistable behaviour for tow-steered laminates," *Composites Part A: Applied Science and Manufacturing*, vol. 43, no. 6, pp. 926–934, 2012.
- [16] B. C. Kim, K. D. Potter, and P. M. Weaver, "Continuous tow shearing for manufacturing variable angle tow composites," *Composites Part A: Applied Science and Manufacturing*, vol. 43, no. 8, pp. 1347–1356, 2012.
- [17] B. C. Kim, P. M. Weaver, and K. D. Potter, "Manufacturing characteristics of the continuous tow shearing method for manufacturing of variable angle tow composites," *Composites Part A: Applied Science and Manufacturing*, vol. 61, pp. 141–151, 2014.
- [18] Z. Gürdal, B. F. Tatting, and K. C. Wu, "Variable stiffness composite panels: Effects of stiffness variation on the in-plane and buckling response," *Composites Part A: Applied Science and Manufacturing*, vol. 39, no. 5, pp. 911–922, 2008.
- [19] R. M. J. Groh and P. M. Weaver, "On displacement-based and mixed-variational equivalent single layer theories for modelling highly heterogeneous laminated beams," *International Journal of Solids and Structures*, vol. 59, pp. 147–170, 2015.
- [20] Z. Wu, G. Raju, and P. M. Weaver, "Buckling of VAT plates using energy methods," in *53rd AIAA/ASME/ASCE/AHS/ASC Structures, Structural Dynamics, and Materials Conference*, no. AIAA-2012-1463, (Honolulu, HI, U.S.A), AIAA, 2012.
- [21] S. P. Timoshenko, *Theory of elasticity*. McGraw-Hill Book Company, 1934.
- [22] E. Reissner, "On the theory of bending of elastic plates," *Journal of Mathematical Physics*, vol. 23, pp. 184–191, 1944.
- [23] R. Mindlin, "Influence of rotatory inertia and shear on flexural motions of isotropic elastic plates," *ASME Journal of Applied Mechanics*, vol. 18, pp. 31–38, 1951.
- [24] C. Libove and S. Batdorf, "A general small-deflection theory for flat sandwich plates," tech. rep., Hampton, VA, U.S.A., 1948.
- [25] D. Dawe and T. Craig, "The vibration and stability of symmetrically-laminated composite rectangular plates subjected to in-plane stresses," *Composite Structures*, vol. 5, pp. 281–307, jan 1986.
- [26] W. Ko and R. Jackson, "Combined compressive and shear buckling analysis of hypersonic aircraft structural sandwich panels," tech. rep., NASA, Hampton, VA, U.S.A., 1991.
- [27] The MathWorks Inc., "MATLAB and statistics toolbox release R2013a."
- [28] A. W. Blom, S. Setoodeh, J. M. Hol, and Z. Gürdal, "Design of variable-stiffness conical shells for maximum fundamental eigenfrequency," *Computers & Structures*, vol. 86, no. 9, pp. 870–878, 2008.
- [29] C. Runge, "Über empirische funktionen und die interpolation zwischen äquidistanten ordinaten," *Zeitschrift für Mathematik und Physik*, vol. 46, no. 20, pp. 224–243, 1901.

- [30] L. Kollár and G. S. Springer, *Mechanics of composite structures*. Cambridge University Press, 2003.
- [31] H. G. Allen, *Analysis and Design of Structural Sandwich Panels*. Pergamon Press, 1969.
- [32] K. Washizu, *Variational methods in elasticity and plasticity*. Pergamon Press, second ed., 1975.
- [33] Hexcel Composites, “HexWeb honeycomb sandwich design technology,” 2000.
- [34] Hysol, “SynCore design guide: an aerospace technology Guide,” 2006.
- [35] J. R. Vinson, “Optimum design of composite honeycomb sandwich panels subjected to uniaxial compression,” *AIAA Journal*, vol. 24, no. 10, pp. 1690–1696, 1986.
- [36] Dassault Systèmes, “ABAQUS 6.12 (2012) documentation,” 2012.
- [37] M. A. Wadee and G. W. Hunt, “Interactively induced localized buckling in sandwich structures with core orthotropy,” *Journal of Applied Mechanics*, vol. 65, no. 2, pp. 523–528, 1998.